Flux-vector model of spin noise in superconducting circuits: Electron versus nuclear spins and role of phase transition

S. LaForest and Rogério de Sousa*

Department of Physics and Astronomy, University of Victoria, Victoria, British Columbia V8W 2Y2, Canada
(Dated: July 22, 2015)

Superconducting Quantum Interference Devices (SQUIDs) and other superconducting circuits are limited by intrinsic flux noise with spectral density $1/f^\alpha$ with $\alpha < 1$ whose origin is believed to be due to spin impurities. Here we present a theory of flux noise that takes into account the vectorial nature of the coupling of spins to superconducting wires. We present explicit numerical calculations of the flux noise power (spectral density integrated over all frequencies) for electron impurities and lattice nuclear spins under several different assumptions. The noise power is shown to be dominated by surface electron spins near the wire edges, with bulk lattice nuclear spins contributing $\sim 5\%$ of the noise power in aluminum and niobium wires. We consider the role of electron spin phase transitions, showing that the spin-spin correlation length (describing e.g. the average size of ferromagnetic spin clusters) greatly impacts the scaling of flux noise with wire geometry. Remarkably, flux noise power is exactly equal to zero when the spins are polarized along the flux vector direction, forming what we call a poloidal state. Flux noise is non-zero for other spin textures, but gets reduced in the presence of correlated ferromagnetic fluctuations between the top and bottom wire surfaces, where the flux vectors are antiparallel. This demonstrates that engineering spin textures and/or inter-surface correlation provides a method to reduce flux noise in superconducting devices.

I. INTRODUCTION

Superconducting Quantum Interference Devices (SQUIDs) are among the most sensitive and useful magnetometers.[1] They are able to detect magnetic fields as low as 10^{-17} Tesla,[2] and are currently used in a wide variety of applications. Examples include outer space tests of general relativity, detection of short-circuit faults in microchips, as well as several applications in medicine, such as measuring regions of brain activity in magneto-encephalography. However, this high degree of sensitivity also causes the SQUIDs to be sensitive to magnetic fluctuations intrinsic to its wires and interfaces.

The most sensitive SQUIDs show excess flux noise (in addition to Johnson-Nyquist white noise) of the order of 1 $\mu\Phi_0/\sqrt{\text{Hz}}$ at a frequency of 1 Hz [$\Phi_0 = h/(2|e|)$ is the flux quantum]. This value has not changed in order of magnitude since the first measurements of flux noise in the 1980's;[3,4] only minor improvements are observed in modern devices.[5–10] While flux noise is sufficiently low for several applications, it is still considered a barrier for the use of the SQUID as a quantum bit (the flux qubit) in a superconductor-based quantum computer architecture.[11] Flux noise induces dephasing and relaxation of flux qubits, limiting their coherence times to less than 20 μs.[12] Flux noise also degrades performance of other superconducting (SC) qubits such as the transmon[13] and phase qubit.[6] The effort to reduce flux noise and increase qubit coherence times has been a major source of motivation for research in improving SC devices.

The flux threading a SQUID at low temperatures was shown to follow the Curie susceptibility law (magnetic susceptibility $\propto 1/T$),[14] supporting the idea that the origin of flux noise was due to the fluctuation of local magnetic moments (presumably spin impurities) near the superconducting wire (Fig. 1).[15–19] The identity of these local moments remains unknown; some of the possibilities are illustrated in Fig. 2, which depicts the longitudinal cross-section of a typical Josephson junction. Candidates for the local moments include a variety of spin species: Dangling-bonds,[16] interface states,[18] adsorbed molecules,[20] and nuclear spins of all atoms forming the materials.[21–24]

Recent theory and experiment[25] provided evidence that low temperature/low frequency SQUID flux noise can be explained by a spin diffusion model, with spin diffusion constant measured to be of the order of 10 μm^2/s.
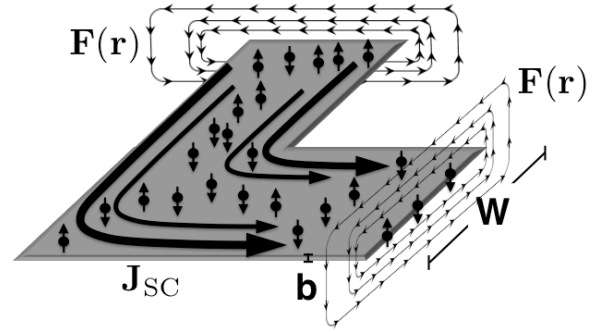

FIG. 1: Section of a superconducting wire with a random distribution of spin impurities. The wire is made of superconducting thin-film of thickness b and lateral width W, with $b \ll W$. The flux Φ_i produced by a spin s_i located at position R_i is given by $\Phi_i = -F(R_i) \cdot s_i$, with flux vector $F(R_i)$ parallel to the magnetic field produced by the supercurrent at R_i.

Interestingly, this value is right in the range of spin diffusion constants measured for lattice nuclear spins due to their mutual dipolar interaction.[26] The typical metals that form superconducting wires (e.g. niobium, aluminum) all have non-zero lattice nuclear spin, that are expected to contribute to intrinsic flux noise up to frequencies of the order of 10^4 Hz (the value of dipolar coupling between nearest-neighbor nuclei in the crystal lattice).[27] Nuclear spin noise should be present even in hypothetically "perfect" devices that contain no electron spin centers.

Recent experiments[13,28] claimed the observation of flux noise at frequencies several orders of magnitude above the nuclear spin cut-off frequency (10^4 Hz). Therefore, nuclear spins alone can not explain the origin of flux noise in SC devices.

Here we describe a theory for the excess flux detected by SC circuits in the presence of localized magnetic moments, and make explicit numerical predictions for the flux noise power (noise spectral density integrated over all frequencies) originating from electron and nuclear spins uniformly distributed in the surface and bulk of the SC wires. Our main assumption is that the superconducting condensate affects the value of the spin's magnetic moment only through local screening described by the London equations. We consider the impact of the formation of spin clusters (spatial spin-spin correlation), which is typical of electron spin systems close to a phase transition.[29,30] This allows the assessment of the relative contributions of surface impurity electrons and bulk lattice nuclear spins in a variety of regimes. We present simple analytic expressions that allow direct comparisons to flux noise models and experiments.

As we shall demonstrate, flux noise power depends crucially on the vectorial nature of the coupling between SC circuit to spins. This vectorial nature can be mapped out by measuring flux noise as a function of the direction and magnitude of an external magnetic field applied along the plane of the wires.

Previous calculations of flux noise due to localized spin[15] were based on modelling the spin as a square loop of side 0.1 μm, the minimum feature size allowed by the finite element software FastHenry.[31] More recently, extensive numerical studies[25,32] showed that these calculations greatly underestimated the value of the flux produced by spins located at the wire surfaces, because they did not take account of the singular nature of the spin's dipole field. Indeed, analytic expressions for the flux noise power that take into account the spin's singular behaviour are still absent from the literature. Below we obtain these expressions and argue that they can be applied to arbitrary circuits made of thin-film wires. We shall show below that our expressions lead to much larger values than previous ones,[6] but are in close agreement with the most recent numerical studies.[32]

The article is organized as follows: Section II introduces our flux-vector model, and develops a general theory on how flux noise depends on flux vector and the
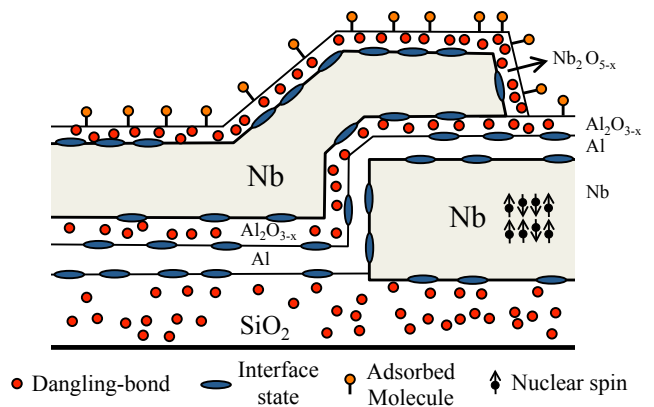

FIG. 2: (color online). Longitudinal cross-section of a typical Josephson junction[7,25] and expected location of the spin species causing flux noise. The superconducting wire is made of niobium, the insulator of partially oxidized aluminum (likely amorphous), and the substrate of silicon-dioxide. Candidates for the spin species include electron and nuclear spins. Amorphous interfaces are well known sources of electron spin centers such as dangling-bonds[16] and interface states.[18] We also depict molecules adsorbed to the surface, that were shown to lead to electron traps.[20] All materials have non-zero lattice nuclear spin that contribute to flux noise even in the absence of defects (e.g. Nb has nuclear spin $S = 9/2$).

formation of spin clusters near a phase transition. Section III describes our numerical dipole method to calculate the flux vector explicitly. Section IV describes our numerical results and compares them to FastHenry calculations. Section V describes numerical results for the noise power due to electron spins distributed in the surface of the wires, with and without spin clustering. Section VI describes our results for spins distributed in the bulk of the wire, with explicit calculations for lattice nuclear spins in aluminum and niobium. Section VII discusses the implications of our results for reducing flux noise and presents our conclusions.

II.   FLUX-VECTOR MODEL

A.   General case

Consider an ensemble of localized spins labelled by $i = 1, \ldots, N$. Each spin is located at position $\boldsymbol{R}_i$, and is described by the spin-S operator $\boldsymbol{s}_i$. This can describe electron or nuclear spins, e.g. single electron impurity centers ($S = 1/2$), many-electron transition metal centers ($S \geq 1/2$), or nuclear spins of lattice atoms such as aluminum ($S = 5/2$) or niobium ($S = 9/2$). We introduce the notion of the flux vector $\boldsymbol{F}_i \equiv \boldsymbol{F}(\boldsymbol{R}_i)$, whose components $F_{i\alpha}$ describe the value of the flux for a spin pointing along direction $\alpha = x, y, z$. The total flux that the spin produces on the wires forming a device is written

as

$$\Phi = -\sum_i \boldsymbol{F}_i \cdot \boldsymbol{s}_i. \tag{1}$$

Note that the $\boldsymbol{F}_i$ are real vectors with dimensions of flux ($\boldsymbol{s}_i$ is assumed dimensionless), and Φ is a scalar quantum operator describing flux. The sign in Eq. (1) ensures $\boldsymbol{F}_i \parallel \boldsymbol{B}(\boldsymbol{R}_i)$, the magnetic field produced by the SC's current density at the spin's location $\boldsymbol{R}_i$ (See Section III below). Such a flux is directly measured in a SQUID, but more generally will couple to any superconducting circuit by producing a voltage $V = -d\Phi/dt$. The problem of flux noise in superconducting circuits is to compute the thermal equilibrium noise spectral density:

$$\tilde{S}_\Phi(f) = \int_{-\infty}^{\infty} dt \; \mathrm{e}^{2\pi i f t} \langle \delta\Phi(t)\delta\Phi(0)\rangle, \tag{2}$$

where $\delta\Phi(t) = \Phi(t) - \langle\Phi\rangle$, with the angular brackets corresponding to thermal average $\langle A \rangle = \mathrm{Tr}\{\rho_T A\}$, with $\rho_T = \mathrm{e}^{-\mathcal{H}/(k_B T)}/Z$ the thermal equilibrium density matrix, $\mathcal{H}$ the spin Hamiltonian, and $Z = \mathrm{Tr}\{\mathrm{e}^{-\mathcal{H}/(k_B T)}\}$ the partition function.

We perform a spectral decomposition of Eq. (2) by formally diagonalizing the spin Hamiltonian, $\mathcal{H}|\alpha\rangle = E_\alpha|\alpha\rangle$:

$$\tilde{S}_\Phi(f) = \sum_{\alpha,\beta} \frac{\mathrm{e}^{-\frac{E_\alpha}{k_B T}}}{Z} |\langle\alpha|\delta\Phi(0)|\beta\rangle|^2 \delta\left(f - \frac{E_\beta - E_\alpha}{h}\right). \tag{3}$$

Any mechanism that couples the spins to the lattice[16] or to themselves[17,25,29] leads to finite frequency noise. However, evaluating Eq. (3) for a large spin system is a challenging task that requires a series of uncontrolled approximations.

The mechanism of frequency dependence in Eq. (3) is a subject of current research. In Ref. 25 the frequency dependence of Eq. (3) was evaluated under the assumption that the spins are in a paramagnetic phase with spin dynamics governed by spin diffusion, leading to $1/f^\alpha$ noise with exponent $0 < \alpha < 1.5$ dependent on frequency range and device geometry. Reference 29 proposed a model based on spin-clusters and non-diffusive dynamics driven by spin-spin dipolar interaction. It was argued that the distribution of cluster sizes gives rise to a large spread of spin-flip times and $1/f^{0.85}$ noise over a broad frequency range, independent of device geometry.

Here we shall focus our discussion on the total flux noise power,

$$\begin{aligned} \left\langle (\delta\Phi)^2 \right\rangle &= \int_{-\infty}^{\infty} \tilde{S}_\Phi(f) df \\ &= \sum_{i,j,\alpha,\beta} F_{i\alpha} F_{j\beta} \left(\frac{1}{2} \langle \{s_{i\alpha}, s_{j\beta}\} \rangle \right. \\ &\qquad\qquad \left. - \langle s_{i\alpha}\rangle\langle s_{j\beta}\rangle \right), \end{aligned} \tag{4}$$

where $\{A, B\} = AB + BA$ denotes the anticommutator of two operators. We note that Eq. (4) is independent

on the particular interaction mechanism driving spin dynamics; thus it allows a model independent comparison of the role of $\boldsymbol{F}$ and the contribution arising from different spin species. We take a continuum limit by introducing the magnetization or spin density

$$\boldsymbol{M}(\boldsymbol{r}) = -\sum_i \boldsymbol{s}_i \delta(\boldsymbol{r} - \boldsymbol{R}_i), \tag{5}$$

and defining the spin-spin spatial correlation function as

$$C^{\alpha\beta}(\boldsymbol{r}, \boldsymbol{r}') = \frac{1}{2} \langle \{M_\alpha(\boldsymbol{r}), M_\beta(\boldsymbol{r}')\} \rangle - \langle M_\alpha(\boldsymbol{r})\rangle \langle M_\beta(\boldsymbol{r}')\rangle. \tag{6}$$

In the continuum limit Eq. (4) becomes

$$\left\langle (\delta\Phi)^2 \right\rangle = \int d^d r \int d^d r' \sum_{\alpha,\beta} F_\alpha(\boldsymbol{r}) C^{\alpha\beta}(\boldsymbol{r}, \boldsymbol{r}') F_\beta(\boldsymbol{r}'), \tag{7}$$

with dimension $d = 2$ (surface) and $d = 3$ (bulk) to be considered below.

The noise power Eq. (7) depends on spin texture through the spatial correlation function $C^{\alpha\beta}(\boldsymbol{r}, \boldsymbol{r}')$. If the spin system is close to a phase transition, noise power will show strong temperature dependence because of the formation of spin clusters, which are described in general by deviations of $C^{\alpha\beta}(\boldsymbol{r}, \boldsymbol{r}')$ from a delta function $\delta(\boldsymbol{r} - \boldsymbol{r}')$. In addition, Eq. (7) may be temperature dependendent even in the absence of spin clusters, as we show below.

B. Noise power without spatial correlation (independent spins)

There are many situations where the correlation function is well approximated by a delta function, and the state of any spin is independent of the others. These include high temperature, spin textures with zero correlation (e.g. spin glass), and when all spins are fully polarized along one direction. Below we consider each case in detail.

In the limit of high temperature, defined by $k_B T$ being much larger than any energy scale affecting the spins, we may carry out a $1/T$ expansion of Eq. (6) and retain only the leading order contribution (zeroth power of $1/T$, which is exact at $T = \infty$). This leading order contribution has all different spin configurations occurring with equal probability, implying $\langle s_{i\alpha}\rangle = 0$ and $\langle s_{i\alpha} s_{j\beta}\rangle = \frac{S(S+1)}{3}\delta_{ij}\delta_{\alpha\beta}$. Further assuming that the spins are uniformly distributed in space with density σ_d leads to

$$C^{\alpha\beta}_{T=\infty}(\boldsymbol{r}, \boldsymbol{r}') = \frac{S(S+1)}{3}\sigma_d \delta(\boldsymbol{r} - \boldsymbol{r}')\delta_{\alpha\beta}, \tag{8}$$

and the high temperature noise power

$$\left\langle (\delta\Phi)^2 \right\rangle_{T=\infty} = \frac{S(S+1)}{3}\sigma_d \int d^d r \, |\boldsymbol{F}(\boldsymbol{r})|^2, \tag{9}$$

which is formally exact at $T = \infty$. In the absence of an external magnetic field, Eq. (9) is a good approximation for nuclear spins down to μK temperatures (the energy scale for nuclear-nuclear dipolar interaction between nearest-neighbor nuclear spins).

If the spin system is in a phase that has approximately zero spatial correlation ($\langle s_{i\alpha} s_{j\beta} \rangle \approx \langle s_{i\alpha} \rangle \langle s_{j\beta} \rangle$ for $i \neq j$), and if they are uniformly distributed in space, the correlation function may be approximated by

$$C_{\text{unc.}}^{\alpha\beta}(\boldsymbol{r}, \boldsymbol{r}') = f^{\alpha\beta}(\boldsymbol{r}, T)\sigma_d \delta(\boldsymbol{r} - \boldsymbol{r}'), \quad (10a)$$

$$f^{\alpha\beta}(\boldsymbol{R}_i, T) = \left[\frac{1}{2} \langle \{s_{i\alpha}, s_{i\beta}\} \rangle - \langle s_{i\alpha} \rangle \langle s_{i\beta} \rangle \right], \quad (10b)$$

leading to the uncorrelated spin noise power

$$\left\langle (\delta\Phi)^2 \right\rangle_{\text{unc.}} = \sigma_d \int d^d r \sum_{\alpha,\beta} F_\alpha(\boldsymbol{r}) f^{\alpha\beta}(\boldsymbol{r}, T) F_\beta(\boldsymbol{r}). \quad (11)$$

This expression is a good approximation in at least three cases of interest: (1) At temperatures higher than the spin-spin coupling J, but lower than single-spin anisotropy energy (which is non-zero for $S > 1/2$). Assuming the single-spin anisotropy is equal for all spins, the function $f^{\alpha\beta}(\boldsymbol{r}, T)$ will depend only on temperature and not on $\boldsymbol{r}$, and will differ from $\delta_{\alpha\beta}$ signaling the presence of anisotropy. (2) At all temperatures, when the spin-spin coupling alternates in sign randomly, such as in a spin-glass. As a result, the coarse-grained spin-spin correlation function will average out to zero over the length scales of $F_\alpha(\boldsymbol{r})$, but the long time averages $\langle s_{i\alpha} \rangle$ will remain non-zero (non-ergodicity). A space-dependent function $f^{\alpha\beta}(\boldsymbol{r}, T)$ may be used to model the lack of translation symmetry of the spin state. In the simpler case of translation symmetry, a spin-diffusion model with $f^{\alpha\beta}(T) = S(S+1)\chi(T)/(3\chi_0)\,\delta_{\alpha\beta}$ [Eq. (9) of Ref. 25] was proposed to describe the frequency and temperature dependence of the spin-glass noise. (3) When all spins are polarized along the same direction, which occurs at low T in a ferromagnetic phase, or in the presence of a large external magnetic field.

To illustrate case (1), consider a model spin Hamiltonian with easy-axis anisotropy along $\hat{\boldsymbol{e}}_\|$, $\mathcal{H}_{\text{ani.}} = -K \sum_i s_{i\|}^2$, with $s_{i\|} = \boldsymbol{s}_i \cdot \hat{\boldsymbol{e}}_\|$ and $K > 0$ the anisotropy energy. When $J \ll k_B T \ll K$ the spins will be equally distributed in the $\pm S$ eigenstates of $s_{i\|}$; after a simple calculation we get $f^{\|,\|} = \langle s_{i\|}^2 \rangle = S^2$ and $f^{\perp 1, \perp 1} = f^{\perp 2, \perp 2} = \langle s_{i\perp 1}^2 \rangle = S/2$, with all other correlations equal to zero, leading to

$$\left\langle (\delta\Phi)^2 \right\rangle_{J \ll k_B T \ll K} \approx \sigma_d \int d^d r \left[S^2 F_\|^2(\boldsymbol{r}) + \frac{S}{2} F_\perp^2(\boldsymbol{r}) \right]. \quad (12)$$

Depending on the direction of $\boldsymbol{F}(\boldsymbol{r})$, the noise power may get reduced or increased in comparison to the high T result Eq. (9).

More generally, the Hermitian matrix $f^{\alpha\beta}(\boldsymbol{r}, T)$ can be diagonalized to find its eigenvectors $\hat{\boldsymbol{f}}_\gamma$ and eigenvalues

$a_\gamma = \langle (\boldsymbol{s}_i \cdot \hat{\boldsymbol{f}}_\gamma)^2 \rangle - \langle (\boldsymbol{s}_i \cdot \hat{\boldsymbol{f}}_\gamma) \rangle^2 \geq 0$. We may establish a general inequality for uncorrelated noise by noting that the largest eigenvalue of $f^{\alpha\beta}$ is smaller than $S(S+1)$ (the eigenvalue of $\boldsymbol{s}_i^2$):

$$\begin{aligned} \left\langle (\delta\Phi)^2 \right\rangle_{\text{unc.}} &= \sigma_d \int d^d r \sum_\gamma a_\gamma \left| \boldsymbol{F}(\boldsymbol{r}) \cdot \hat{\boldsymbol{f}}_\gamma \right|^2 \\ &\leq 3 \left\langle (\delta\Phi)^2 \right\rangle_{T=\infty}. \end{aligned} \quad (13)$$

If $S = 1/2$ and the spin state has translation symmetry, a_γ will be equal to $1/4$ for all γ, and the noise power is simply equal to the $T = \infty$ result Eq. (9).

Finally, we consider case (3) in detail. At low T, the spins may spontaneously polarize if the spin-spin interaction is ferromagnetic (See section II C); alternatively they can be polarized with a strong external magnetic field. Measuring flux noise in the presence of a strong B field is a quite challenging experiment. For superconductivity to remain unaffected, the external B field has to be applied along the plane of all wire segments, with the magnetic length remaining larger than the thin-film width b. Moreover, any modulation of the critical current due to the presence of flux perpendicular to the Josephson junctions will have to be accounted for. Despite these challenges, we shall show that it is worth considering this experiment because it would provide a mapping of $\boldsymbol{F}(\boldsymbol{r})$ and the measurement of spin quantum number S.

When the Zeeman energy scale dominates, the spin Hamiltonian can be approximated by $\mathcal{H}_{\text{Zeeman}} = -\sum_i \boldsymbol{\mu}_i \cdot \boldsymbol{B}$, with $\boldsymbol{\mu}_i = -g\mu_s \boldsymbol{s}_i$. Here we use $\mu_s = \mu_B$ for electron spins (μ_B is the Bohr magneton), and $\mu_s = -\mu_N$ for nuclear spins (μ_N is the nuclear magneton), with g the g-factor (g is quite close to 2 for most electron impurities but can be very different than 2 for nuclei). In this regime correlation between different spins will be zero and the functions $f^{\alpha\beta}(\boldsymbol{r}, T)$ in Eq. (10b) can be separated into two kinds, $f_\|(T)$ and $f_\perp(T)$:

$$\begin{aligned} f_\|(\tilde{B}) &= \langle (\boldsymbol{s}_i \cdot \hat{\boldsymbol{B}})^2 \rangle - \langle (\boldsymbol{s}_i \cdot \hat{\boldsymbol{B}}) \rangle^2 \\ &= \frac{1}{4} \left\{ \frac{1}{\sinh^2(\tilde{B})} - \frac{(2S+1)^2}{\sinh^2[(2S+1)\tilde{B}]} \right\}, (14a) \\ f_\perp(\tilde{B}) &= \langle (\boldsymbol{s}_i \cdot \hat{\boldsymbol{B}}_{\perp 1})^2 \rangle = \langle (\boldsymbol{s}_i \cdot \hat{\boldsymbol{B}}_{\perp 2})^2 \rangle \\ &= \frac{1}{4} \coth(\tilde{B}) \left\{ (2S+1) \coth[(2S+1)\tilde{B}] \right. \\ &\quad \left. - \coth(\tilde{B}) \right\}, \end{aligned} \quad (14b)$$

where $\hat{\boldsymbol{B}}$ is the unit vector along the magnetic field, $\hat{\boldsymbol{B}}_{\perp 1}, \hat{\boldsymbol{B}}_{\perp 2}$ is a set of orthogonal unit vectors perpendicular to it, and $\tilde{B} = g\mu_s B/(2k_B T)$ measures the strength of the field. The equilibrium spin polarization is given by

$$\langle \boldsymbol{s}_i \rangle = -\frac{1}{2} \{ (2S+1) \coth[(2S+1)\tilde{B}] - \coth(\tilde{B}) \} \hat{\boldsymbol{B}}. \quad (15)$$

Plugging these expressions into Eq. (11) yields

$$\left\langle (\delta\Phi)^2 \right\rangle_{\text{High } B} \approx \sigma_d \int d^d r \left[f_\perp \left| \boldsymbol{F}(\boldsymbol{r}) \right|^2 - (f_\perp - f_\parallel) \left| \boldsymbol{F}(\boldsymbol{r}) \cdot \hat{\boldsymbol{B}} \right|^2 \right]. \quad (16)$$

Since $f_\perp(\tilde{B}) > f_\parallel(\tilde{B})$ for all $\tilde{B}$, Eq. (16) shows that the noise power *gets reduced upon the application of external B field.* In the limit $\tilde{B} \gg 1$, all spins are polarized leading to

$$\left\langle (\delta\Phi)^2 \right\rangle_{\text{pol.}\parallel\hat{\boldsymbol{B}}} = \frac{S}{2}\sigma_d \int d^d r \left[\left| \boldsymbol{F}(\boldsymbol{r}) \right|^2 - \left| \boldsymbol{F}(\boldsymbol{r}) \cdot \hat{\boldsymbol{B}} \right|^2 \right], \quad (17)$$

which is quite different from the high T result Eq. (9). Equation (17) is the *exact noise power of a fully polarized spin system*, irrespective of whether the polarization occurs because of application of a B field, or due to spontaneous symmetry breaking e.g. in a ferromagnetic ground state. Thus, measurements of the dependence of noise as a function of the direction and magnitude of the in-plane magnetic field, or on direction of the spin polarization provides information on the components of the flux vector $\boldsymbol{F}(\boldsymbol{r})$ and on the value of the spin quantum number S.

As we show below, the direction of $\boldsymbol{F}(\boldsymbol{r})$ is poloidal along the surface of the wire (Fig. 1), implying that *spin polarization along a single direction* can never completely suppress flux noise. Note how the residual noise arises due to the quantum nature of the spins. For example, if the spins are polarized along $\hat{\boldsymbol{x}}$, they have equal probability of pointing along any of the four directions $+\hat{\boldsymbol{y}}, -\hat{\boldsymbol{y}}, +\hat{\boldsymbol{z}}, -\hat{\boldsymbol{z}}$. This uncertainty gives rise to quantum noise power proportional to $F_{iy}^2 + F_{iz}^2$.

Finally, consider a spin-polarized state where each spin located at $\boldsymbol{R}_i$ points parallel or antiparallel to $\boldsymbol{F}_i$; we call this the poloidal state. The noise power produced by this state is obtained by evaluating the average in Eq. (4) with a single product state of N spins each pointing along $\boldsymbol{F}_i$; the result is identical to Eq. (17) with $\hat{\boldsymbol{B}} \to \hat{\boldsymbol{F}}(\boldsymbol{r})$, leading to

$$\left\langle (\delta\Phi)^2 \right\rangle_{\text{Poloidal}} = 0. \quad (18)$$

Therefore, engineering the poloidal spin texture enables complete suppression of flux noise. We emphasize that this is an exact result; it happens because in the poloidal state every single spin quantum fluctuation has to be perpendicular to $\boldsymbol{F}_i$, producing zero flux noise.

C. Noise power with spatial correlation (ferromagnetic spin clusters)

The interaction between the spins may lead to non-zero spatial correlation. To see the impact on flux noise power,
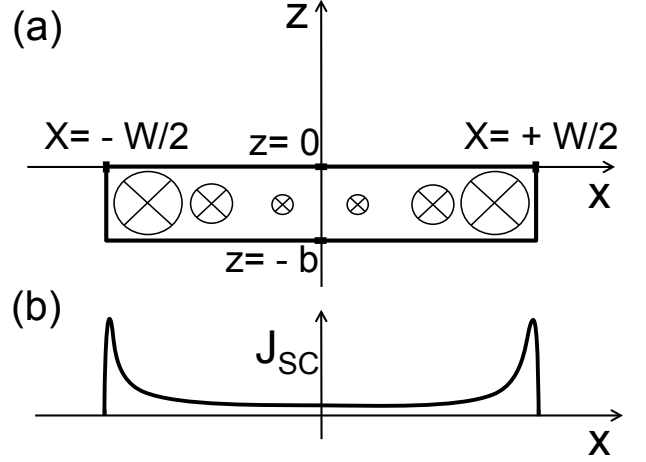

FIG. 3: (a) Transverse cross-section of the SQUID wire (See also Fig. 1). The current density is shown pointing along the y-direction. (b) Magnitude of the superconductor current density as a function of x [Eq. (33)].

consider the Heisenberg model with easy-axis anisotropy,

$$\mathcal{H}_{\text{s-s}} = -\frac{1}{2} \sum_{i,j} J(\boldsymbol{R}_i - \boldsymbol{R}_j)\boldsymbol{s}_i \cdot \boldsymbol{s}_j - K \sum_i s_{i\parallel}^2, \quad (19)$$

where $K \geq 0$ and $s_{i\parallel} = \boldsymbol{s}_i \cdot \hat{\boldsymbol{e}}_\parallel$, with $\hat{\boldsymbol{e}}_\parallel$ the direction of the anisotropy axis. We take the continuum limit with $\boldsymbol{M}(\boldsymbol{r})$ as in Eq. (5), and expand Eq. (19) up to the second order in spatial derivatives:

$$\mathcal{H}_{\text{s-s}} \approx \int d^d r \left\{ \frac{\bar{J}\xi_0^d}{2} \left[-|\boldsymbol{M}|^2 + \xi_0^2 \sum_{\alpha=x,y,z} |\nabla M_\alpha|^2 \right] - \frac{K}{\sigma_d} M_\parallel^2 \right\}. \quad (20)$$

This expression is valid in the long-wavelength approximation, when terms of order $|\nabla^2 M|^2$ are negligible.

The exchange interaction is assumed to satisfy

$$\int d^d r J(\boldsymbol{r}) x_\alpha x_\beta = 2\xi_0^{d+2} \bar{J} \delta_{\alpha\beta}, \quad (21)$$

with parameters ξ_0 and $\bar{J}$ defined by

$$\xi_0^2 = \frac{1}{2} \frac{\int d^d r J(\boldsymbol{r}) x_\alpha^2}{\int d^d r J(\boldsymbol{r})}, \quad (22a)$$

$$\bar{J} = \frac{1}{\xi_0^d} \int d^d r J(\boldsymbol{r}). \quad (22b)$$

Parameter ξ_0 models the range of the exchange interaction, while $\bar{J}$ models its average strength. Many competing interactions contribute to $J(\boldsymbol{r})$, such as direct exchange (always antiferromagnetic) and RKKY (ferromagnetic when $k_F|\boldsymbol{R}_i - \boldsymbol{R}_j| \ll 1$).[17,29,30] We shall focus

(a)Spin pointing along x (along the wire surface)

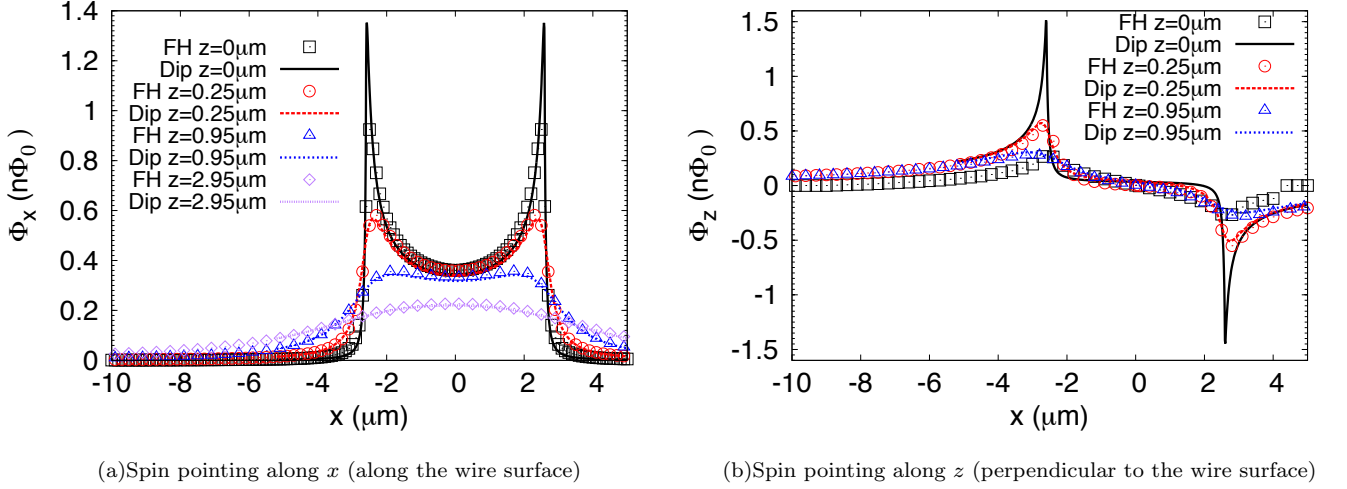(b)Spin pointing along z (perpendicular to the wire surface)

FIG. 4: (color online). Comparison of the Flux produced by each spin as a function of spin location calculated by FastHenry and the numerical dipole method, for a superconducting wire of penetration depth $\lambda = 0.07\ \mu$m, thickness $b = 0.1\ \mu$m, and width $W = 5.2\ \mu$m. The coordinate x runs along the lateral width of the wire, with edges at $x = \pm 2.6 \mu$m.

in the case $0 < \bar{J} < \infty$ and $\xi_0 < \infty$, when the system is able to transition into a ferromagnetic state with $\boldsymbol{M} \parallel \pm \hat{\boldsymbol{e}}_\parallel$. We shall also use Eq. (20) with a space-dependent $\hat{\boldsymbol{e}}_\parallel = \hat{\boldsymbol{F}}(\boldsymbol{r})$ as a toy model that we call the *poloidal model*. When $K \gg \bar{J}\sigma_d\xi_0^d(\xi_0/b)^2$ such a model has the poloidal state $\boldsymbol{M}(\boldsymbol{r}) \parallel \pm \boldsymbol{F}(\boldsymbol{r})$ as its $T = 0$ ground state.

We use mean-field theory;[33] this is done by subtracting T times the single spin entropy from Eq. (20). The result is that the system develops a ferromagnetic moment $\langle M_\parallel \rangle \neq 0$ at the critical temperature

$$k_B T_c = \frac{S(S+1)}{3}\left(\sigma_d\xi_0^d\bar{J} + 2K\right), \qquad (23)$$

with correlation functions given by:

$$C^{\parallel,\parallel}(\boldsymbol{r},\boldsymbol{r}') = \frac{k_B T}{\bar{J}\xi_0^{d+2}}\int \frac{d^d q}{(2\pi)^d}\frac{e^{i\boldsymbol{q}\cdot(\boldsymbol{r}-\boldsymbol{r}')}\xi_\parallel^2}{1+\left(\xi_\parallel q\right)^2}, (24a)$$

$$C^{\perp\alpha,\perp\beta}(\boldsymbol{r},\boldsymbol{r}') = \frac{k_B T}{\bar{J}\xi_0^{d+2}}\int \frac{d^d q}{(2\pi)^d}\frac{e^{i\boldsymbol{q}\cdot(\boldsymbol{r}-\boldsymbol{r}')}\xi_\perp^2}{1+\left(\xi_\perp q\right)^2}$$
$$\times \delta_{\alpha\beta}, \qquad (24b)$$

where $\perp \alpha$ with $\alpha = 1,2$ denote the two directions perpendicular to $\hat{\boldsymbol{e}}_\parallel$ (the correlation function between $\parallel$ and $\perp \alpha$ is zero). There are two correlation length scales $\xi_\parallel$

and $\xi_\perp$:

$$\xi_\parallel(T) = \xi_0\sqrt{\frac{T'}{u_T|T - T_c|}}, \qquad (25a)$$

$$\xi_\perp(T > T_c) = \xi_0\sqrt{\frac{T'}{(T - T')}}, \qquad (25b)$$

$$\xi_\perp(T < T_c) = \xi_0\sqrt{\frac{\sigma_d\xi_0^d\bar{J}}{2K}}, \qquad (25c)$$

where $k_B T' = [S(S+1)/3]\sigma_d\xi_0^d\bar{J}$ and $u_T = 1$ for $T > T_c$ and $u_T = 2$ for $T < T_c$. The length scales $\xi_\parallel, \xi_\perp$ describe the average size for spin clusters polarized along $\hat{\boldsymbol{e}}_\parallel$, and the direction perpendicular to it, respectively. Note $T_c > T'$, so that only $\xi_\parallel$ diverges at the transition. For $d = 2$ we get

$$C^{\parallel,\parallel}_{d=2}(\boldsymbol{r} - \boldsymbol{r}') = \frac{k_B T}{2\pi\bar{J}\xi_0^4}K_0\left(\frac{|\boldsymbol{r} - \boldsymbol{r}'|}{\xi_\parallel}\right), \qquad (26a)$$

$$C^{\perp\alpha,\perp\beta}_{d=2}(\boldsymbol{r} - \boldsymbol{r}') = \frac{k_B T}{2\pi\bar{J}\xi_0^4}K_0\left(\frac{|\boldsymbol{r} - \boldsymbol{r}'|}{\xi_\perp}\right)\delta_{\alpha\beta}, (26b)$$

where $K_0(x)$ is the modified Bessel function of the 2nd kind.

The noise power for surface spins ($d = 2$) in the presence of correlations is obtained by plugging Eqs. (26a), (26b) into Eq. (7), leading to

$$\frac{\left\langle(\delta\Phi)^2\right\rangle_{\text{corr.}}}{\left\langle(\delta\Phi)^2\right\rangle_{T=\infty}} = \frac{T}{u_T|T - T_c|}\frac{\int d^2r \int d^2r' \left[F_\parallel(\boldsymbol{r})F_\parallel(\boldsymbol{r}')K_0\left(\frac{|\boldsymbol{r}-\boldsymbol{r}'|}{\xi_\parallel}\right) + \boldsymbol{F}_\perp(\boldsymbol{r})\cdot\boldsymbol{F}_\perp(\boldsymbol{r}')K_0\left(\frac{|\boldsymbol{r}-\boldsymbol{r}'|}{\xi_\perp}\right)\right]}{2\pi\xi_\parallel^2\int d^2r|\boldsymbol{F}(\boldsymbol{r})|^2}, \qquad (27)$$

where we presented correlated noise divided by the $T = \infty$ uncorrelated noise [Eq. (9)] for convenience. Notably, Eq. (27) depends on model parameters only through $\xi_\parallel, \xi_\perp$ and T_c. Once again, the vector nature of $\boldsymbol{F}(\boldsymbol{r})$ plays an important role in determining noise power: Correlated noise tends to decrease (increase) when $\boldsymbol{F}(\boldsymbol{r})$ and $\boldsymbol{F}(\boldsymbol{r}')$ are antiparallel (parallel) for $\boldsymbol{r}, \boldsymbol{r}'$ in different surfaces of the wire (See e.g. the top and bottom wire surfaces in Fig. 1).

We remark that mean-field theory neglects critical fluctuations and is not necessarily a good approximation for T close to T_c. For $d = 1, 2$ and $K = 0$ (or $S = 1/2$, when easy-axis anisotropy is effectively zero), critical fluctuations reduce the actual T_c of the Heisenberg model to zero.[34] For $K > 0$, T_c is generally non-zero at $d = 2$, but can be substantially reduced in comparison to the mean-field prediction Eq. (23). However, *mean-field theory is an excellent approximation in the region $T \gg T_c$, when critical fluctuations play no role.* To see this, consider the $T \gg T_c$ limit of Eqs. (25a)–(26b): We get $\xi_\parallel, \xi_\perp \approx \xi_0 \sqrt{T'/T} \to 0$, and $K_0(|\boldsymbol{r} - \boldsymbol{r}'|/\xi) \to 2\pi\xi^2 \delta(\boldsymbol{r} - \boldsymbol{r}')$, leading to $C^{\alpha\beta}(\boldsymbol{r} - \boldsymbol{r}') \approx k_B T'/(\bar{J}\xi_0^2)\delta(\boldsymbol{r} - \boldsymbol{r}')\delta_{\alpha\beta}$. Plugging $k_B T' = [S(S+1)/3]\sigma_d \xi_0^d \bar{J}$ we see that this is identical to the $T = \infty$ limit shown in Eq. (8).

Furthermore, mean-field theory neglects quantum fluctuations; this is a problem for the $T \ll T_c$ region, where mean-field theory is exact only in the limit $S \to \infty$. When $J(\boldsymbol{R}_i - \boldsymbol{R}_j) > 0$ for all i, j, the exact $T = 0$ state of the system will have all spins fully polarized along either $+\hat{\boldsymbol{e}}_\parallel$ or $-\hat{\boldsymbol{e}}_\parallel$ (or an arbitrary direction for $S = 1/2$) leading to

$$C^{\parallel,\parallel}_{T=0}(\boldsymbol{r}, \boldsymbol{r}') = 0, \tag{28a}$$

$$C^{\perp\alpha,\perp\beta}_{T=0}(\boldsymbol{r}, \boldsymbol{r}') = \frac{S}{2}\sigma_d \delta(\boldsymbol{r} - \boldsymbol{r}')\delta_{\alpha\beta}. \tag{28b}$$

Hence $C^{\perp\alpha,\perp\alpha}(\boldsymbol{r}, \boldsymbol{r}')$ remains non-zero when $T \to 0$, signaling the presence of quantum fluctuations. Plugging Eqs. (28a), (28b) into Eq. (7) we get the spin polarized noise Eq. (17) with $\hat{\boldsymbol{B}} = \hat{\boldsymbol{e}}_\parallel$. While this result disagrees with mean-field theory, we note that the ratio of Eq. (17) to Eq. (9) is proportional to $1/(S + 1)$. When $S \to \infty$ this ratio goes to zero, in agreement with the $T \to 0$ limit of Eq. (27).

III. EVALUATION OF THE FLUX VECTOR: THE NUMERICAL DIPOLE METHOD

When an electron travels across a closed path $\mathcal{C}$ inside the SC wire, it is affected by a flux equal to $\Phi_i = \int_{\mathcal{C}} \boldsymbol{A}_i(\boldsymbol{r}) \cdot d\boldsymbol{l}$, where $\boldsymbol{A}_i(\boldsymbol{r})$ is the vector potential for the spin $\boldsymbol{s}_i$ located at $\boldsymbol{R}_i$. For an extended wire with SC current density $\boldsymbol{J}_{SC}(\boldsymbol{r})$ and total current I_{SC}, the corresponding flux can be obtained by representing the wire by

a set of infinitesimally thin closed paths $\mathcal{C}$, and summing over all the paths with $d\boldsymbol{l} = d^3r \boldsymbol{J}_{SC}(\boldsymbol{r})/I_{SC}$, a weighting factor that represents the fraction of current flowing through each path:

$$\Phi_i = \int d^3r \boldsymbol{A}_i(\boldsymbol{r}) \cdot \boldsymbol{J}_{SC}(\boldsymbol{r}), \tag{29}$$

where the integral is over the region where $\boldsymbol{J}_{SC} \neq 0$, i.e. the volume of the wire. The numerical dipole method consists in using the spin-dipole expression for $\boldsymbol{A}_i(\boldsymbol{r})$,[35]

$$\boldsymbol{A}_i(\boldsymbol{r}) = -\frac{g\mu_s\mu_0}{4\pi} \frac{\boldsymbol{s}_i \times (\boldsymbol{r} - \boldsymbol{R}_i)}{|\boldsymbol{r} - \boldsymbol{R}_i|^3}, \tag{30}$$

together with an analytical approximation for $\boldsymbol{J}_{SC}(\boldsymbol{r})$. Plugging Eq. (30) into Eq. (29) we get $\Phi_i = -\boldsymbol{F}(\boldsymbol{R}_i) \cdot \boldsymbol{s}_i$ with

$$\boldsymbol{F}(\boldsymbol{R}) = \frac{g\mu_s\mu_0}{4\pi} \int d^3r \frac{(\boldsymbol{r} - \boldsymbol{R}) \times \boldsymbol{J}_{SC}(\boldsymbol{r})}{|\boldsymbol{r} - \boldsymbol{R}|^3 I_{SC}} \tag{31a}$$

$$= \frac{g\mu_s\mu_0}{4\pi} \nabla_{\boldsymbol{R}} \times \left[\int d^3r \frac{\boldsymbol{J}_{SC}(\boldsymbol{r})}{I_{SC} |\boldsymbol{r} - \boldsymbol{R}|} \right]. \tag{31b}$$

Note that we choose a sign convention so that $\boldsymbol{F}(\boldsymbol{R})$ points along $\boldsymbol{B}(\boldsymbol{R})$, the magnetic field produced by $\boldsymbol{J}_{SC}$ at $\boldsymbol{R}$, and that the direction of $\boldsymbol{F}$ can be found using the right hand rule with the thumb pointing towards $\boldsymbol{J}_{SC}$ (Fig. 1). The corresponding Zeeman energy of the spin system is given by $\mathcal{H}_{Zeeman} = -I_{SC} \int d^dr \boldsymbol{F}(\boldsymbol{r}) \cdot \boldsymbol{M}(\boldsymbol{r})$. We remark that this same result can be obtained from the flux-inductance theorem.[36]

The current density $\boldsymbol{J}_{SC}$ includes contributions from external sources plus screening currents causing Meissner effect. To find $\boldsymbol{J}_{SC}$ one usually has to integrate the London equations numerically with the help of software packages such as FastHenry.[31] However, there exists an important case where $\boldsymbol{J}_{SC}$ is known analytically: Thin-film wires of width $b \lesssim \lambda$, where λ is the SC penetration depth ($\lambda = 0.05 - 0.1 \mu$m for most superconductors), and wire lateral width W that is large enough to satisfy

$$\tilde{\lambda} \equiv \frac{\lambda^2}{bW} \ll 1, \tag{32}$$

and $\xi_{SC} \ll W$, where ξ_{SC} is the superconductor coherence length including the electron mean free path (this latter condition ensures that the London equations with a single length scale λ is a good approximation).

Below we present analytic results in terms of powers of the small parameter $\tilde{\lambda}$. Neglecting terms that are first order in $\tilde{\lambda}$, the SC wire current density can be written as[37,38]

(a)Spin pointing along x (along the wire surface)

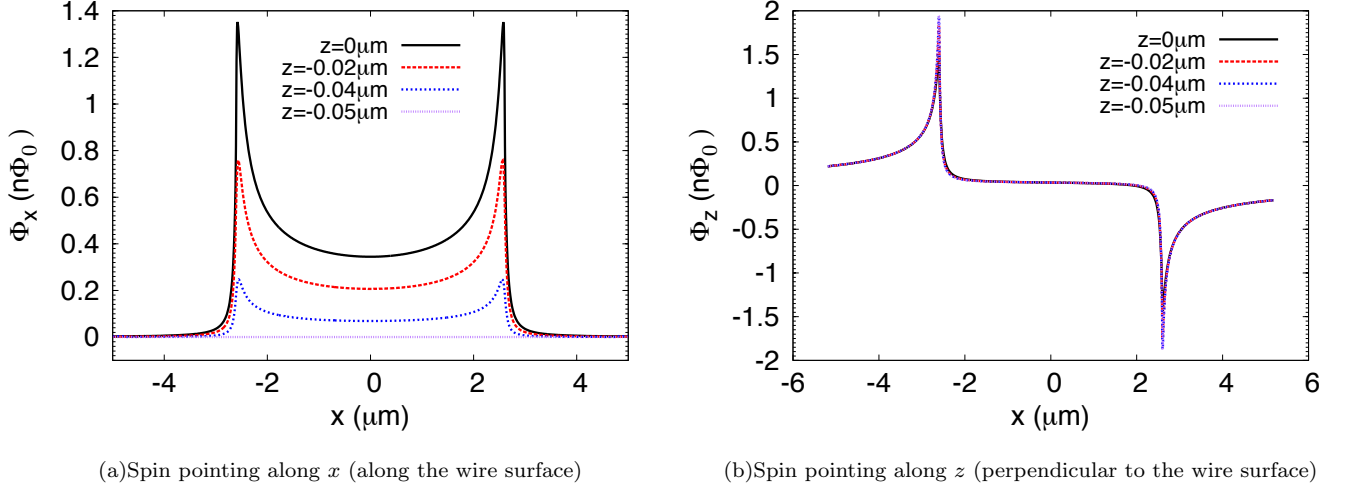(b)Spin pointing along z (perpendicular to the wire surface)

FIG. 5: (color online). Flux produced by an electron spin impurity as a function of spin location inside the SC wire. All results used the numerical dipole method, for a superconducting wire of penetration depth $\lambda = 0.07$ μm, thickness $b = 0.1$ μm, and width $W = 5.2$ μm. The coordinate x runs along the lateral width of the wire, with edges at $x = \pm 2.6 \mu$m. Note how the flux is zero in the region inside the wire ($z = -b/2$ and x away from the edges).

$$\boldsymbol{J}_{\text{SC}}(\boldsymbol{r}) = \frac{2 I_{SC}}{\pi b W \left(1 - \gamma \sqrt{2\tilde{\lambda}}\right)} \boldsymbol{\hat{y}} \begin{cases} \frac{1}{\sqrt{2\tilde{\lambda}}} e^{-\frac{(1 - \tilde{\lambda} - |u|)}{2\tilde{\lambda}}} & \text{for } (1 - \tilde{\lambda}) < |u| \leq 1, \\ \frac{1}{\sqrt{1 - u^2}} & \text{for } |u| \leq (1 - \tilde{\lambda}), \end{cases} \tag{33}$$

where $\gamma = 2(2 - e^{1/2})/\pi = 0.2236$ is a numerical constant, and the coordinate $u = 2x/W$ runs along the lateral width of the wire, as shown in Fig. 3. The numerical dipole method consists in using Eq. (33) in Eq. (31b) to get an approximation for the flux vector *that neglects the feedback effect of the spins on* $\boldsymbol{J}_{\text{SC}}$. This feedback effect shall not be significant when the spins are unpolarized. Later we will confirm this expectation by comparing our numerical dipole method to exact integration of the London equations using FastHenry, and show that non-zero spin polarization leads to an asymmetry on top of this solution.

It is straightforward to integrate Eq. (31b) explicitly for the infinitely long wire with coordinate axes shown in Fig. 3. For a spin located at $\boldsymbol{R} = (X, 0, Z)$,

$$F_x(X, Z) = -\frac{g \mu_s \mu_0 W}{8\pi} \int_{-1}^{1} du \frac{J_{\text{SC}}(u)}{I_{\text{SC}}} \ln \left[\frac{(x - X)^2 + Z^2}{(x - X)^2 + (Z + b)^2} \right], \tag{34a}$$

$$F_y(X, Z) = 0, \tag{34b}$$

$$F_z(X, Z) = \frac{g \mu_s \mu_0 W}{4\pi} \int_{-1}^{1} du \frac{J_{\text{SC}}(u)}{I_{\text{SC}}} \left[\arctan \left(\frac{Z + b}{x - X} \right) - \arctan \left(\frac{Z}{x - X} \right) \right]. \tag{34c}$$

We can integrate a few particular cases analytically; neglecting terms that are first order in $\tilde{\lambda}$:

- *Mid-surface,* $(X = 0, Z = 0)$:

$$F_x \approx \frac{g \mu_s \mu_0}{\pi W} \left[\frac{1 - \gamma \frac{b}{W} \sqrt{2\tilde{\lambda}}}{1 - \gamma \sqrt{2\tilde{\lambda}}} \right], \tag{35a}$$

$$F_z = 0. \tag{35b}$$

This expression is a good approximation in the top surface away from the wire edge. For electrons with $g = 2$, and assuming $\sqrt{2\tilde{\lambda}} \ll 1$ we get $|\boldsymbol{F}_{\text{mid-surface}}| \approx \left(\frac{3.6 \mu m}{W} \right) n \Phi_0$ ($n\Phi_0 = 10^{-9} \Phi_0$).

- *Mid-edge, $(X = \frac{W}{2}, Z = -\frac{b}{2})$:*

$$F_x = 0, \tag{36a}$$

$$F_z \approx -\frac{g\mu_s\mu_0}{\pi\sqrt{bW}\left(1 - \gamma\sqrt{2\tilde{\lambda}}\right)}\left[1 - \gamma\frac{\lambda/b}{\sqrt{1 + 2\left(\frac{\lambda}{5b}\right)^2}}\right]. \tag{36b}$$

- *Corner, $(X = \frac{W}{2}, Z = 0)$:*

$$F_x \approx \frac{g\mu_s\mu_0}{\pi\sqrt{2bW}\left(1 - \gamma\sqrt{2\tilde{\lambda}}\right)}\left\{1 - \tanh\left[\frac{1}{2}\sqrt{\frac{\lambda}{b}}\right]\right\}, \tag{37a}$$

$$F_z \approx -\frac{g\mu_s\mu_0}{\pi\sqrt{2bW}\left(1 - \gamma\sqrt{2\tilde{\lambda}}\right)}\left[1 - \frac{\gamma}{\sqrt{2}}\frac{(\lambda/b)}{\sqrt{1 + \left(\frac{\lambda}{5b}\right)^2}}\right]. \tag{37b}$$

Note how $\boldsymbol{F}_i$ close to the wire edge is sensitive to the ratio λ/b. The mid-edge case, Eq. (36b) provides the maximum $|\boldsymbol{F}_i|$ for a single electron spin interacting with a thin-film wire. When $\lambda/b \lesssim 1$, $|\boldsymbol{F}_{\text{edge}}| \approx \left(\frac{3.6\mu\text{m}}{\sqrt{bW}}\right) n\Phi_0$. However, when $\lambda/b \gg 1$ (ultra-thin wires), the edge flux can be reduced by as much as a factor of three.

At the edge, the associated local field produced by the SQUID's current on the spin is at most $|\boldsymbol{B}_{\text{loc}}| = \mu_0 I_{\text{SC}}/(\pi\sqrt{bW})$. For typical $I_{\text{SC}} \sim 1$ mA and $\sqrt{bW} \sim 1$ μm we get $|\boldsymbol{B}_{\text{loc}}| \sim 4$ Gauss, that is not sufficient to polarize electron spins even at the lowest temperatures achieved in the laboratory (10 mK). In SQUIDs made of carbon nanotubes or other nanostructures, the value of single-spin flux and the local field can be much larger.[39]

IV. NUMERICAL RESULTS AND COMPARISON TO FINITE LOOP APPROXIMATION/FASTHENRY

We now present explicit numerical calculations of the flux vector by numerical integration of Eqs. (34a)–(34c). In order to validate our numerical dipole method, we performed comparison calculations using the finite loop/FastHenry method of Refs. 15, 32. We did this by designing a FastHenry[31] input file that included a long SC wire representing the SQUID, and a small square loop of side 0.1 μm representing the spin. FastHenry has the advantage of integrating the London equations exactly.

Figure 4(a) shows the computed $\Phi_X \equiv F_x/2$ (value of flux for spin-1/2 pointing along x) for electron spins interacting with a SC wire of penetration depth $\lambda = 0.07$ μm, thickness $b = 0.1$ μm, and lateral width $W = 5.2$ μm. The flux is plotted as a function of spin location X (along the lateral width as in Fig. 3). Each curve was calculated for a different spin-wire surface distance Z. Note how the numerical dipole calculations are right on top of the FastHenry results for $Z \leq 0.25$ μm. However,

for $Z = 0$ the numerical dipole results are 50% larger. Figure 4(b) shows the results for $\Phi_z \equiv F_z/2$ (flux for spin-1/2 pointing along z, perpendicular to the wire surface). Again, we see that both calculation methods agree for $Z \leq 0.25$ μm. However, at $Z = 0$ (wire surface) we find that the numerical dipole method gives a flux that is *six times larger* than FastHenry.

Figure 5 shows the numerical dipole results for electron spins inside the wire (negative Z). While the flux is quite high at the wire surface, it decreases to zero inside the wire ($Z = -b/2$ and X away from the edges). This result is particularly relevant for nuclear spins, as it shows that nuclei inside the wire give a smaller contribution to flux noise (single nuclear spin flux is $\sim 10^3$ times smaller than the single electron values shown in the figure).

It is important to note that all calculations presented here assumed a SC wire of infinite length. As a result, the flux at the wire edges (at $x = \pm W/2$) are of identical magnitude, i.e., the flux is symmetric with respect to $X = 0$. Actual devices will show some degree of asymmetry for the current densities at the wire edges. For example, the SQUID is a closed SC wire loop, so to satisfy the Meissner effect it produces higher current density at the inside wire edge,[32] thus minimizing the value of magnetic field inside the wire. Modifying Eq. (33) to include this asymmetry would lead to the same degree of asymmetry in the calculated flux vectors.

Another source of asymmetry in $\boldsymbol{J}_{\text{SC}}$ occurs due to spin polarization in applied B fields. With $\boldsymbol{B}$ pointing along $\hat{\boldsymbol{x}}$, the superconductor will generate a current difference δI_{SC} between the top and bottom wire surfaces, in order to screen out the magnetic moment generated by polarized spins. A simple estimate is given by $|\delta I_{\text{SC}}|Lb = |\mu_B|N$, with $N \approx 2\sigma_2 LW$ the number of spins at the top+bottom surfaces. This leads to $|\delta I_{\text{SC}}| \sim 2\mu_B\sigma_2 W/b \sim 10 - 1000$ μA for $b = 0.1$ μm and $W = 1 - 100$ μm.

While these asymmetries can be significant, they do not seem to modify the noise power results shown in the

(a)Top surface, spin at $(X, 0, 0)$ or at $(X, 0, -b)$
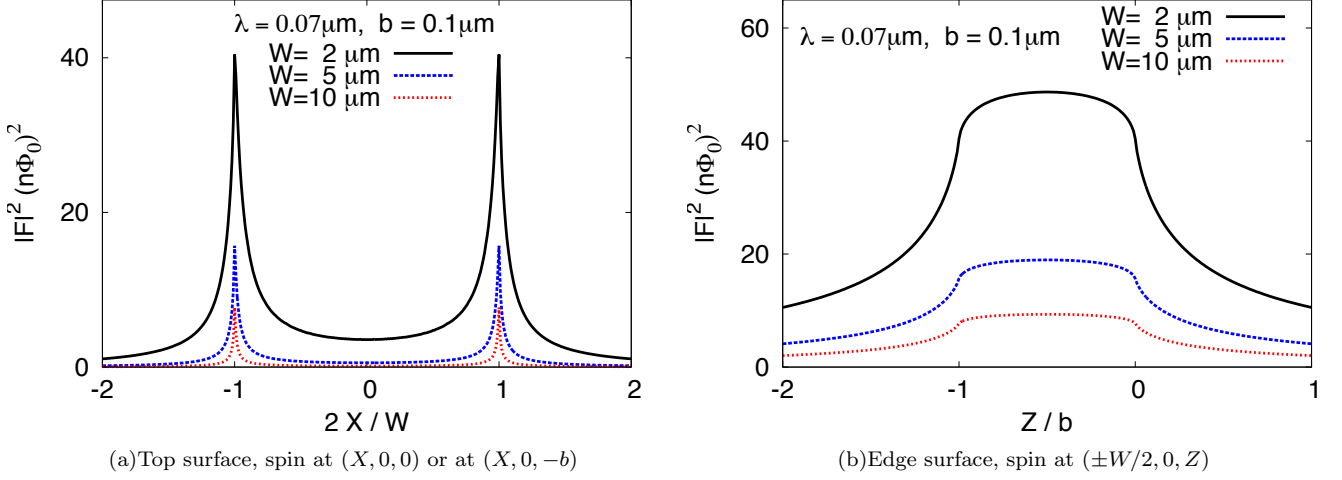
(b)Edge surface, spin at $(\pm W/2, 0, Z)$

FIG. 6: (color online). Flux vector squared for electron spin at the top and edge surfaces of the wire, for $\lambda = 0.07$ μm, $b = 0.1$ μm and $W = 2, 5, 10$ μm. The coordinate X runs along the lateral width of the top surface, while Z runs along the side surface. Note how the flux is sharply peaked near the wire edges.
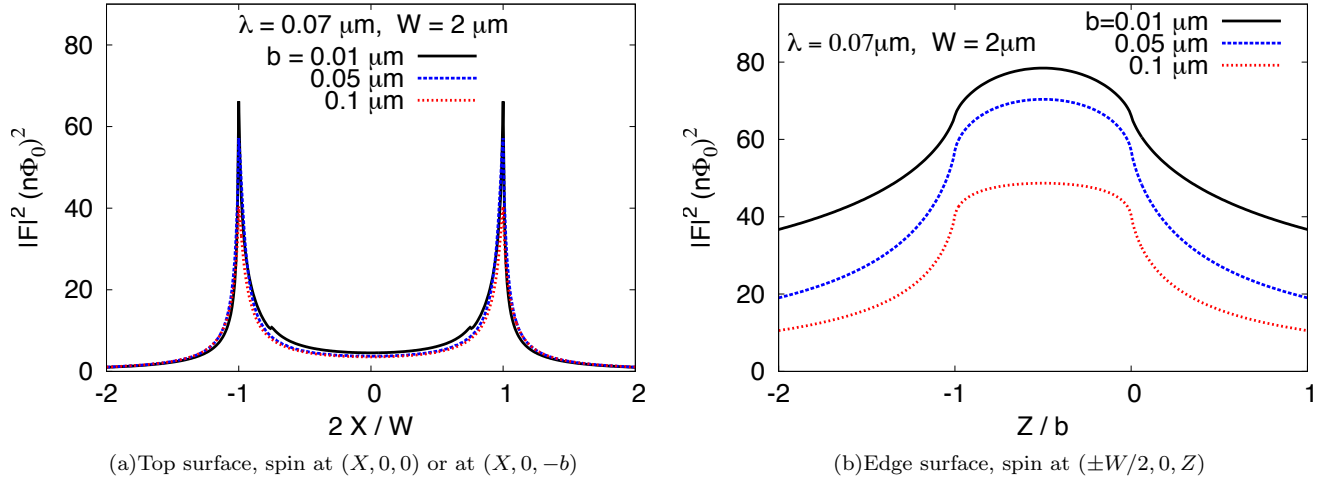

(a)Top surface, spin at $(X, 0, 0)$ or at $(X, 0, -b)$

(b)Edge surface, spin at $(\pm W/2, 0, Z)$

FIG. 7: (color online). Flux vector squared for electron spin at the top and edge surfaces of the wire, for $\lambda = 0.07$ μm, $W = 2$ μm, and different wire thickness b. Note how the edge flux is quite sensitive to b.

next section. This occurs because $\langle (\delta\Phi)^2 \rangle$ is an integral of $|\boldsymbol{F}|^2$ over all wire surfaces; since the asymmetry increases the current in one region and decreases it by the same amount in another, the asymmetry cancels out in computations of the noise power summed over all surfaces.

V. FLUX NOISE POWER FOR SURFACE SPINS

We will now present results for flux noise power in a single wire with length L, width W, and thickness b. Our results can be applied to devices that contain more wires by simply adding the noise power contributed by each

wire segment.

A. Without spatial correlation, no spin clusters

Here we focus our discussion in the $T = \infty$ noise power with $S = 1/2$ [Eq. (9)]. We recall that this constitutes the exact noise power for $S = 1/2$ in the absence of spatial correlation and space inhomogeneity (See section II B); and for $S > 1/2$ it can be multiplied by $4S(S + 1)$ to yield an upper bound on the uncorrelated noise at all temperatures [Eq. (13)].

Figures 6-8 show explicit calculations of $|\boldsymbol{F}|^2$ for electrons located at the top and edge wire surfaces for a
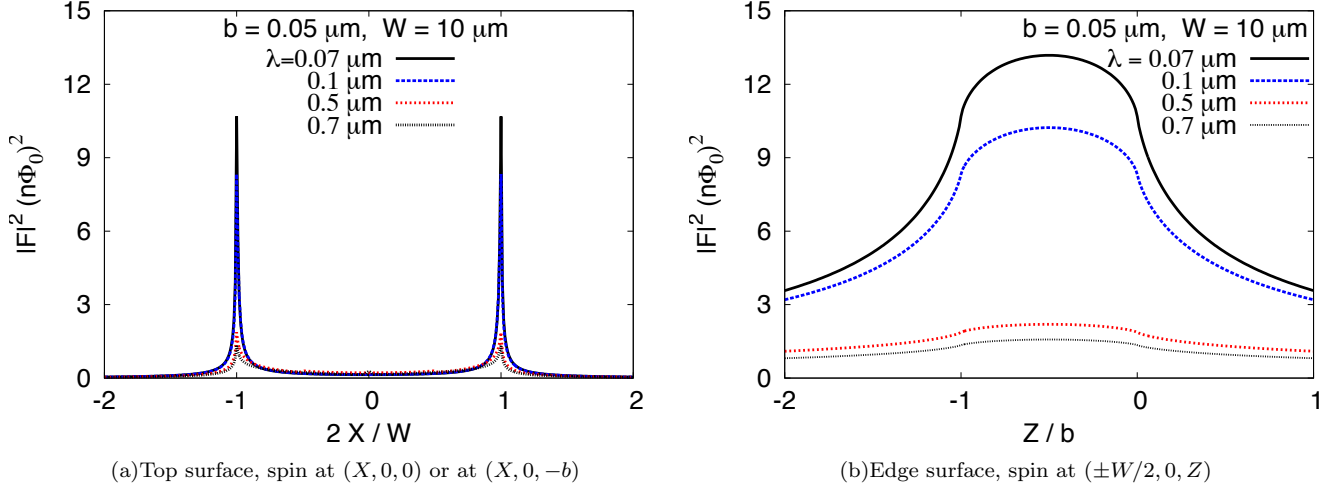
(a)Top surface, spin at $(X, 0, 0)$ or at $(X, 0, -b)$

(b)Edge surface, spin at $(\pm W/2, 0, Z)$

FIG. 8: (color online). Flux vector squared for electron spin at the top and edge surfaces of the wire, for $W = 10$ μm, $b = 0.05$ μm, and different penetration depth λ. Note how the edge flux is quite sensitive to λ.

range of parameters. Here we see the extent to which flux noise power is sharply peaked at $X = \pm W/2$ for all wire geometries.

The noise power due to surface electrons in a single wire with length L is evaluated by assuming a uniform area density of electrons σ_2 and plugging $S = 1/2$ in Eq. (9):

$$
\begin{aligned}
\langle \Phi^2 \rangle_{\text{Top Surf.}} &= \frac{1}{4} \sigma_2 L \int_{-W/2}^{W/2} dX |\boldsymbol{F}|^2 \\
&\approx \frac{\frac{5}{16\pi^2} (g\mu_s\mu_0)^2 \left(\frac{W}{2b}\right)^{1/4} \left(\frac{\sigma_2 L}{W}\right)}{\left(1 - \gamma\sqrt{2\tilde{\lambda}}\right)^2 \left[1 + 2\left(\frac{2b}{W}\right)^2\right]^{1/4}} \\
&= \frac{4.05 \left(\frac{W}{2b}\right)^{1/4} \left[\frac{\sigma_2 L(\mu\text{m})}{W}\right] (n\Phi_0)^2}{\left(1 - \gamma\sqrt{2\tilde{\lambda}}\right)^2 \left[1 + 2\left(\frac{2b}{W}\right)^2\right]^{1/4}}, (38)
\end{aligned}
$$

where in the second line we approximated the exact result by an analytic expression (good within 1% for $10^{-3} < 2b/W < 1$), and in the third line we assumed $g\mu_s = 2\mu_B$. We find that the top surface noise power is to a good approximation independent of λ. The reason for this can be seen in Fig. 8(a), where it is shown that $|\boldsymbol{F}|^2$ only depends on λ when X is extremely close to $\pm W/2$ (Note how the peak value increases with decreasing λ, but the peak width remains small). As a result we find that the λ-dependent contribution to Eq. (38) is always small.

The edge contribution is quite different. Figures 6(b)-8(b) show that it is a good approximation to assume $|\boldsymbol{F}|^2$ constant for all Z/b, with its value given by Eq. (36b)

squared. Hence we get:

$$
\begin{aligned}
\langle \Phi^2 \rangle_{\text{Edge Surf.}} &\approx \frac{1}{4} \sigma_2 L b |\boldsymbol{F}_{\text{edge}}|^2 \\
&= \frac{(g\mu_s\mu_0)^2}{4\pi^2} \left(\frac{\sigma_2 L}{W}\right) \left(\frac{1 - \gamma\frac{\lambda/b}{\sqrt{1 + 2\left(\frac{\lambda}{5b}\right)^2}}}{1 - \gamma\sqrt{2\tilde{\lambda}}}\right)^2 \\
&= 3.24 \left[\frac{\sigma_2 L(\mu\text{m})}{W}\right] \left(\frac{1 - \gamma\frac{\lambda/b}{\sqrt{1 + 2\left(\frac{\lambda}{5b}\right)^2}}}{1 - \gamma\sqrt{2\tilde{\lambda}}}\right)^2 \\
&\quad \times (n\Phi_0)^2. \quad (39)
\end{aligned}
$$

Comparing Eq. (39) to Eq. (38) we see that in a typical device (satisfying $W < 10^3 b$), the edge surface contribution has the same order of magnitude as the top surface contribution. Flux noise measurements in several niobium SQUIDs[25] were fitted to spin-diffusion theory to yield $\sigma_2 = 5 \times 10^{12}$ cm^{-2}, leading to noise power Eqs. (38) and (39) in the range of $1 - 100$ $(\mu\Phi_0)^2$, see Fig. 12.

Our expressions for the noise power account for the spin-dipole singularity fully, giving values that are qualitatively different and numerically much larger than other expressions derived in the literature. For example, Eq. (6) of Ref. 6 predicted a term proportional to $\ln(\tilde{\lambda})$ in the top surface electron noise power of a circular SQUID; in contrast, our results show that the top noise power is roughly independent of $\tilde{\lambda}$, with the edge noise strongly dependent on λ/b.

We now compare our results to the state of the art numerical calculations of noise power in SQUID washers presented in Anton et al.[32] Our Eq. (9) is larger than Eq. (1) of Ref. 32 by a factor of $S(S + 1)/S^2$, which equals 3 for $S = 1/2$. After multiplying the results

of Ref. 32 by 3, we find that our $\langle\Phi^2\rangle_{\text{Top+bottom}}$ (obtained after adding-up 4 wire segments forming a washer) is 10% smaller than theirs for the case of short wires ($L \sim 10 \ \mu\text{m}$) in a wide range of parameters. For longer wires ($L \sim 100 \ \mu\text{m}$), we find that our results are as much as 40% smaller. This quite good agreement indicates that corner effects are not substantial.

B. With spatial correlation, ferromagnetic spin clusters

We now present explicit numerical results of noise power with ferromagnetic correlations, for the case of surface electrons. In order to evaluate Eq. (27) we separate each surface integral into the 4 surfaces making the wire:

$$\int d^2r = \int_{\text{Top}} d^2r + \int_{\text{Bottom}} d^2r + \int_{\text{EdgeR}} d^2r + \int_{\text{EdgeL}} d^2r. \quad (40)$$

The total integral $\int d^2r \int d^2r'$ breaks up into 16 contributions, of which only 5 are distinct: $2\times$Top-Top (because Bottom-Bottom is identical to Top-Top by symmetry), $2\times$EdgeR-EdgeR, $8\times$Top-Edge, $2\times$Top-Bottom, and $2\times$EdgeL-EdgeR. For ferromagnetic correlations the first 3 are always positive, while the last two are always negative.

Figure 9 shows calculations of the correlated noise power Eq. (27) divided by the $T = \infty$ uncorrelated noise Eq. (9) (this ratio is denoted corr./uncorr.), as a function of T/T_c, for anisotropy energy $K/(\sigma_2\xi_0^2\bar{J}) = 0.1$ along the easy-axis $\hat{\boldsymbol{e}}_\parallel = \hat{\boldsymbol{z}}$ (as $T \to 0$ all spins will polarize along $\hat{\boldsymbol{e}}_\parallel$). The correlated noise power has a sharp peak at $T = T_c$; within mean-field theory this peak is finite, and has its width and height governed by the exchange interaction range ξ_0. Quite interestingly, for $\xi_0 \gg b$ the correlated noise can be several orders of magnitude smaller than uncorrelated noise in all regimes, including the $T_c \ll T \ll \infty$ regime where mean-field theory is known to be accurate.

To shed light in this feature, Fig. 10(a) shows correlated noise for $T \gg T_c$, as a function of $\xi_\parallel \approx \xi_\perp \equiv \xi$. Here we see that the origin of the noise reduction is the presence of spin clusters (non-zero spatial correlation). *Remarkably, correlated noise is always smaller than uncorrelated noise for all average cluster sizes ξ.* Figure 10(b) explains the origin of the reduction: For $\xi > b$, the negative Top-Bottom contribution (with $\boldsymbol{F}$ antiparallel) is activated, which nearly cancels out the Top-Top contribution when $\xi \gg b$. Thus, antiparallel $\boldsymbol{F}$ for surfaces across from each other make inter-surface ferromagnetic fluctuations interfere *destructively* with the intra-surface ferromagnetic fluctuations, leading to a reduction of flux noise.

While uncorrelated noise scales roughly as $\sigma_2 L/W$,[6,15] correlated noise shows different behavior governed by the additional length scales ξ. In the "short-range order" regime $b \ll \xi \ll W$, correlated noise scales instead as
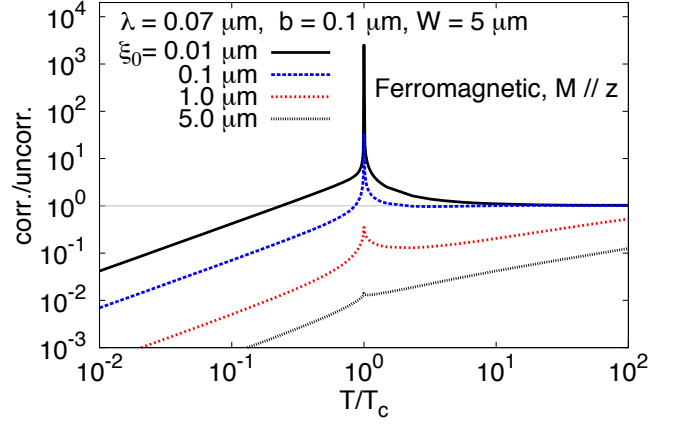

FIG. 9: (color online). Effect of a ferromagnetic phase transition on flux noise power, calculated using mean-field theory with anisotropy energy $K/(\sigma_2\xi_0^2\bar{J}) = 0.1$ along easy axis $\hat{\boldsymbol{e}}_\parallel = \hat{\boldsymbol{z}}$. The ratio of correlated noise to $T = \infty$ noise is shown as a function of T/T_c, calculated from Eq. (27). At $T \approx T_c$ a sharp finite peak appears, with linewidth and peak value depending on ξ_0, the range of the exchange interaction. For large ξ_0, correlated noise can be several orders of magnitude smaller than the $T = \infty$ noise in the region $T_c \ll T < \infty$, suggesting a new method to reduce flux noise in SC devices. The noise reduction occurs due to ferromagnetic correlation between the top and bottom surfaces with antiparallel $\boldsymbol{F}$.

$\hat{\boldsymbol{e}}_\parallel$	corr./uncorr. at $T = 0$
$\hat{\boldsymbol{x}}$	$0.44/(S+1)$
$\hat{\boldsymbol{y}}$	$1.5/(S+1)$
$\hat{\boldsymbol{z}}$	$1.1/(S+1)$

TABLE I: Exact flux noise [from Eq. (17)] for the spin-polarized ground state for three spin polarization directions $\hat{\boldsymbol{e}}_\parallel$. We assumed a long wire with $\boldsymbol{J}_{SC} \parallel \hat{\boldsymbol{y}}$ and other coordinates as in Fig. 3. The zero point flux fluctuation goes to zero only in the classical limit $S \to \infty$.

$\sigma_2 L\lambda/(\xi b)$; in the "long-range order" regime with $\xi \gg W$ it scales as $\sigma_2 L\lambda W/(b\xi^2)$.

When $T \ll T_c$ the spins are polarized along $\hat{\boldsymbol{e}}_\parallel$ leading to pure quantum fluctuation noise that is larger than the mean-field theory prediction. At $T = 0$ the noise can be calculated exactly using Eq. (17) for $\hat{\boldsymbol{B}} = \hat{\boldsymbol{e}}_\parallel$ leading to the values calculated in Table I.

As noted in Eq. (17), flux noise is exactly zero for the poloidal state. We now describe the flux noise power as a function of T for the poloidal model, which comprises Eq. (20) with $\hat{\boldsymbol{e}}_\parallel(\boldsymbol{r}) = \hat{\boldsymbol{F}}(\boldsymbol{r})$ [as noted above this model has the poloidal state as its ground state when $K \gg \bar{J}\sigma_d\xi_0^d(\xi_0/b)^2$]. The resulting correlation functions are formally identical to Eqs. (26a) and (26b); however, they describe correlations between $\hat{\boldsymbol{e}}_\parallel$ directions that are different in different surfaces (we take $\hat{\boldsymbol{e}}_{\perp 1} = \hat{\boldsymbol{y}}$ and $\hat{\boldsymbol{e}}_{\perp 2} = \hat{\boldsymbol{F}}(\boldsymbol{r}) \times \hat{\boldsymbol{y}}$). For example, M_x in the top sur-

(a)Total ratio for different W

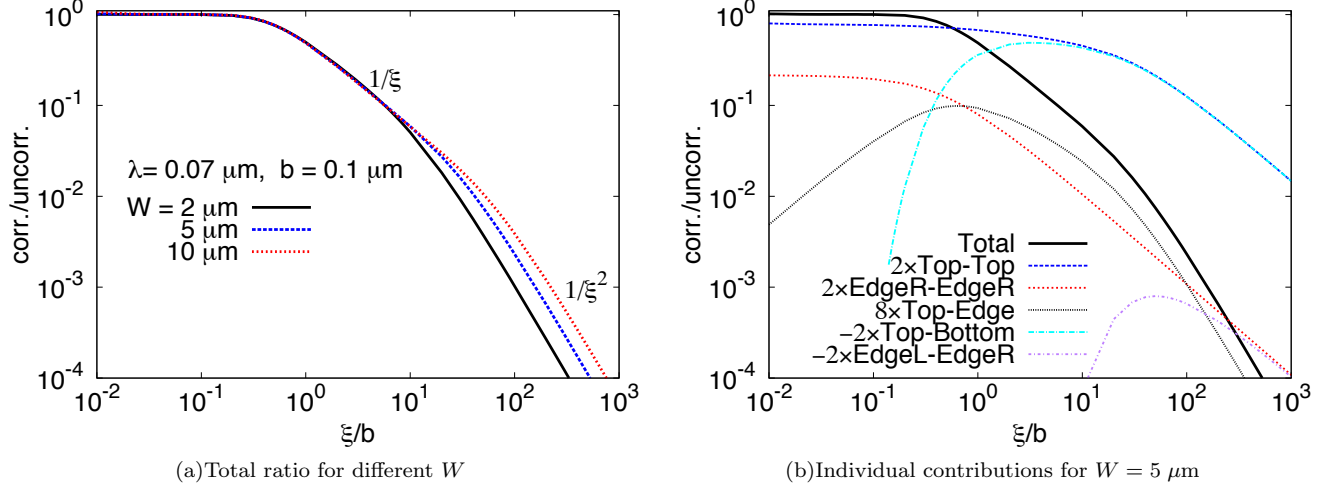(b)Individual contributions for $W = 5\ \mu m$

FIG. 10: (color online). Noise power for the ferromagnetic model with $\hat{\boldsymbol{e}}_\parallel = \hat{\boldsymbol{z}}$ (same as Fig. 9) in the $T \gg T_c$ regime. (a) Correlated noise power divided by uncorrelated noise power (at $T = \infty$). The results are presented as a function of average spin cluster size $\xi_\parallel \approx \xi_\perp \equiv \xi$ divided by wire thickness b. Note how the presence of ferromagnetic spin clusters makes the correlated/uncorrelated ratio smaller than one in the $T_c \ll T < \infty$ regime. The origin of this effect is explained in (b), where each contribution is labelled by a pair of surfaces; for example, $-2\times$Top-Bottom refers to the negative of Top-Bottom + Bottom-Top contribution in Eq. (27). When $\xi > b$, ferromagnetic spin-spin correlation between the wire's top and bottom surfaces (where $\boldsymbol{F}$ is antiparallel) is activated, reducing correlated noise power to a value below the $T = \infty$ uncorrelated noise. When $\xi > W$, ferromagnetic correlation between wire corners (where $\boldsymbol{F}$ is also antiparallel) is activated, producing further reduction of correlated noise.

face is correlated to $-M_z$ in the edge right surface, and to $-M_x$ in the bottom surface. As a consequence, the poloidal model shows antiferromagnetic correlation between spins located in surfaces across from each other, with ferromagnetic correlations between spins located in the same surface. The resulting flux noise power as a function of T/T_c is shown in Fig. 11. The behavior of the poloidal model is seen to be quite distinct from the case of pure ferromagnetic correlation. The noise at $T \approx T_c$ is more than 100 times larger, and at $T > T_c$ correlated flux noise power is *always larger* than the $T = \infty$ uncorrelated case. Clearly, this occurs because for $\xi > b$ the antiferromagnetic inter-surface correlated fluctuations interfere *constructively* with the intra-surface ferromagnetic fluctuations; a simple consequence of having antiparallel $\boldsymbol{F}$ between surfaces across from each other. In contrast to the behavior shown in Figs. 10(a,b) noise power *increases* with increasing spin correlation length ξ. When $T > T_c$ and $b \ll \xi \ll W$, correlated noise scales as $\sigma_2 L \lambda \xi / b^3$; in the "long-range order" regime with $\xi \gg W$ it saturates at its maximum value proportional to $\sigma_2 L \lambda / b^2$.

VI.   BULK NUCLEAR SPINS

For bulk lattice spins inside the wire Eq. (9) becomes

$$\langle \Phi^2 \rangle_{\text{Bulk}} = \frac{S(S+1)}{3} \sigma_3 \int_{\text{wire}} d^3 r \left| \boldsymbol{F}(\boldsymbol{r}) \right|^2, \qquad (41)$$

with the integral running over the volume of the wire, and σ_3 the corresponding volume density for spins. We evaluated this expression numerically and were able to fit the following expression with high accuracy in the region $10^{-3} < 2b/W < 1$:

$$\langle \Phi^2 \rangle_{\text{Bulk}} \approx \frac{S(S+1)}{6\pi^4} \left(g \mu_s \mu_0 \right)^2 \left(\frac{\sigma_3 L W}{b} \right) \frac{\ln \left[1 + \left(\frac{4b}{W} \right)^2 \right]}{\left(1 - \gamma \sqrt{2\tilde{\lambda}} \right)^2}. \qquad (42)$$

Like the case of top surface noise, Eq. (42) is independent of λ because at the edge $\boldsymbol{F}^2$ depends on λ only in a very small fraction of the wire volume. This dependence becomes negligible after volume integration.

We present numerical results for bulk nuclear spins in the typical superconductors aluminum and niobium. For aluminum, the ^{27}Al isotope is 100% abundant in nature, has $S = 5/2$ and $g = 1.46$,[40] and forms a fcc lattice with lattice parameter 4.05 Å. Thus, $\sigma_3 = 4/(4.05\ \text{Å})^3 = 6.02 \times 10^{10}\ \mu\text{m}^{-3}$, and from Eq. (42) we get

$$\langle \Phi^2 \rangle_{\text{Al}} = 1.8 \times 10^{-2} \left[\frac{LW}{b(\mu m)} \right] \frac{\ln \left[1 + \left(\frac{4b}{W} \right)^2 \right]}{\left(1 - \gamma \sqrt{2\tilde{\lambda}} \right)^2} (\mu \Phi_0)^2. \qquad (43)$$

For niobium, the ^{93}Nb isotope is 100% abundant in natural samples, with $S = 9/2$ and $g = 1.37$,[41] and forms a bcc lattice with parameter 3.30 Å leading to
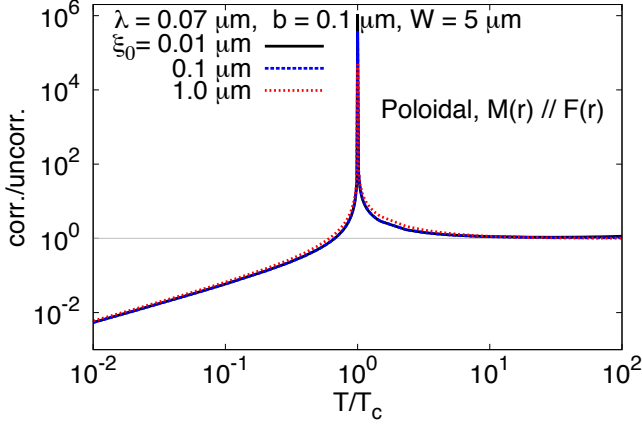
FIG. 11: (color online). Flux noise power of the poloidal model [Eq. (20) with $\hat{e}_{\parallel}(\boldsymbol{r}) = \hat{\boldsymbol{F}}(\boldsymbol{r})$] with anisotropy energy $K/(\sigma_2 \xi_0^2 \bar{J}) = 100$. The ratio of correlated noise to $T = \infty$ noise is shown as a function of T/T_c, calculated from Eq. (27). At $T > T_c$ flux noise is always larger than its $T = \infty$ value, in contrast to the result shown for the ferromagnetic phase (Fig. 9). This occurs because the poloidal model has antiferromagnetic correlation between the top and bottom surfaces. At $T = 0$ the poloidal state has zero flux noise [Eq. (18)] similar to the result obtained in mean-field theory. Engineering the spin system to be close to the poloidal phase provides a novel method to reduce flux noise in SC devices.

$\sigma_3 = 2/(3.30 \text{ Å})^3 = 5.56 \times 10^{10} \ \mu m^{-3}$. We get

$$\langle \Phi^2 \rangle_{\text{Nb}} = 4.2 \times 10^{-2} \left[\frac{LW}{b(\mu m)} \right] \frac{\ln\left[1 + \left(\frac{4b}{W}\right)^2\right]}{\left(1 - \gamma\sqrt{2\tilde{\lambda}}\right)^2} (\mu\Phi_0)^2. \tag{44}$$

The Nb noise power is 2.3 times larger than Al.

Figure 12 compares the $T = \infty$ surface electron and nuclear spin contributions for a Nb wire loop with $L = 100 \ \mu m$, $b = 0.1 \ \mu m$, and $\sigma_2 = 5 \times 10^{12} \ \text{cm}^{-2}$. It shows that the contribution of bulk nuclear spins to the flux noise power is typically 5% of the total noise, that is dominated by surface electrons close to the wire edges.

VII. DISCUSSION AND CONCLUSION

We proposed a flux-vector model of flux noise due to spins in superconducting devices, and performed explicit numerical calculations of the flux noise power produced by localized electron and nuclear spins. We emphasized the crucial difference between electron impurities and lattice nuclear spins. Electron impurities are typically concentrated in the wire surface (where flux vector $\boldsymbol{F}$ is maximum), and can be substantially affected by the formation of spin textures above or below the critical temperature for a spin phase transition. Nuclear spins are instead distributed in the bulk of the wire, and their noise is well described by the $T = \infty$ limit.
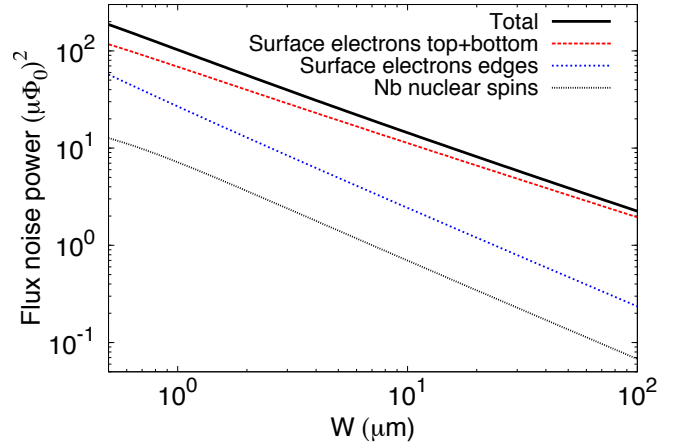

FIG. 12: (color online). Contributions to the $T = \infty$ flux noise power due to surface electrons and nuclear spins, for a niobium wire loop with length $L = 100 \ \mu m$, penetration depth $\lambda = 0.07 \ \mu m$, and thickness $b = 0.1 \ \mu m$, as a function of wire lateral width W. For the surface electrons, we assumed spin area density $\sigma_2 = 5 \times 10^{12} \ \text{cm}^{-2}$ (as measured in Ref. 25), and separated the contributions into top+bottom surfaces and inner+outer side surfaces. The nuclear spin contirbution is for Nb; the noise for Al would be 2.3 times smaller.

In many cases the vectorial nature of the spin-wire coupling plays an essential role in determining the value of the noise power. This includes the case of a phase transition, when additional correlation length scales appear in the problem (describing the average size of spin clusters). Even in the absence of a phase transition the vector nature of $\boldsymbol{F}$ plays a role, e.g. for spins with easy-axis anisotropy (typical of $S > 1/2$ transition metal impurities). The key experiment to directly verify the vectorial nature of $\boldsymbol{F}$ is to measure flux noise in SQUIDs as a function of the magnitude and in-plane direction of an applied magnetic field. Fields of 0.5 Tesla at temperatures of 0.1 K will polarize electron spins without affecting nuclear spins. Table I compares values of flux noise power for large $\boldsymbol{B}$ applied along different directions. Fits using Eq. (16) plus a field independent contribution will allow measurement of S and disentanglement of electron and nuclear spin contributions. These are quite challenging measurements, but we hope they will be performed in the future to confirm the origin of flux noise in superconducting devices.

Our explicit calculations of $\boldsymbol{F}$ for thin-film superconducting wires shows that the flux at the wire edges is much larger than anticipated by previous calculations[6,15,16] because of two reasons. First, the singularity associated to the spin-dipolar field enhances the flux at the wire edges; second, the edge surfaces of thin-film wires (hitherto ignored in previous calculations) contributes the same order of magnitude as the top + bottom surfaces. As a result, the scaling relations for flux as a function of wire geometry are modified. Flux noise can be greatly reduced by minimizing the electron spin

density at the wire edge region. One might be able to achieve this with chemical passivation of the surface[16,20] or by growing the wires with layer by layer deposition (to reduce the number of vacancies and other defects) instead of the usual evaporation method.

We also presented for the first time a realistic estimate for the noise power contributed by nuclear spins. Nuclear spin flux noise has been a subject of speculation for several years,[15,21–24] and we can now ascertain that it accounts for approximately 5% of the total flux noise power affecting typical superconducting devices made with aluminum or niobium. In the future, it is conceivable that one will be able to design SQUIDs with much lower defect spin density, making lattice nuclear spins the ultimate source of noise to be optimized. Nuclear spin noise spectral density ranges from 0 Hz up to $\sim 10^4$ Hz, the value of nearest neighbor spin-spin dipolar interaction. For very thin wires ($2b/W \ll 1$), nuclear spin noise will scale proportional to bL/W, so that further reduction can be achieved by reducing b, L and increasing W. Another alternative would be to use materials with zero lattice nuclear spin, such as making the superconducting wires with lead (Pb). Natural lead samples have 77.9% of zero-nuclear-spin isotopes (^{204}Pb, ^{206}Pb, and ^{208}Pb), with nuclear spin $S = 1/2$ present in only 22.1% (^{207}Pb). Hence, a dramatic reduction in nuclear spin noise is predicted for natural Pb wires. Nuclear spin noise can also be reduced in niobium by using metastable nuclear states such as ^{93m}Nb, the first excited state of ^{93}Nb (100% natural abundance). ^{93m}Nb has $S = 1/2$ with a half-life of 16 years,[42] providing noise reduction by a factor of $(\frac{1}{2} \times \frac{3}{2})/(\frac{9}{2} \times \frac{11}{2}) = \frac{1}{33}$.

For electron spins, a critical experimental question is whether and how flux noise power depends on temperature. The proper answer to this question should reveal whether or not the spin system is close to a phase transition. So far two experiments addressed this question, reaching opposite conclusions in different temperature ranges. Ref. 8 measured a change of up to 10^3 in SQUID flux noise power when the temperature changed from $0.1 - 4$ K; in contrast, Ref. 25 made a direct measurement of noise power in the lower temperature range $0.01 - 0.1$ K (see their Fig. 3), and concluded that there was no change within experimental error bars. It should be noted that even in the absence of a phase transition the noise power may be temperature dependent. This can occur because of spin anisotropy [Eq. (12)] or because $\boldsymbol{F}(\boldsymbol{r})$ is temperature-dependent at temperatures near the superconducting critical temperature [when penetration depth λ increases with temperature and Eq. (32) no longer holds]. The latter effect might be contributing to the temperature dependence observed in Ref. 8.

Our results provide guidance on how to reduce flux noise in SQUIDs and superconducting qubits by changing the wire geometry and/or engineering a spin phase transition. Our Fig. 12 confirms the original claim[6,15] that uncorrelated noise scales roughly as $\sigma_2 L/W$, and can be greatly reduced by using wider wires with larger W. However, in the presence of spin-spin correlation the geometrical scaling of noise is quite different due to the introduction of the spin cluster length scales ξ.

We make several predictions for flux noise power in the presence of magnetic correlation. If the spins at the top surface couple ferromagnetically (antiferromagnetically) to the spins at the bottom surface, flux noise power gets reduced (increased) when the correlation length scale ξ is increased. We should mention that magnetic coupling across thin metallic surfaces is a well established phenomenon in the physics of normal metals sandwiched between ferromagnetic layers. For example, Ref. 43 demonstrates that the RKKY interaction can induce magnetic coupling that alternates back and forth between antiferromagnetic and ferromagnetic depending on the thickness and electron density of the normal metal layer. Perhaps in the future we will be able to engineer SC wires with similar alternation between ferro and antiferro couplings, allowing the corresponding control over flux noise induced by electron spin impurities at the wire surface.

Moreover, we predict that flux noise power is exactly equal to zero for the poloidal spin texture (all spins $\boldsymbol{s}_i$ polarized parallel or antiparallel to their corresponding flux vector $\boldsymbol{F}_i$). This occurs because at $T = 0$ spin fluctuation is perpendicular to the spin polarization axis, which for the poloidal texture is perpendicular to $\boldsymbol{F}_i$ by design; as a result magnetic fluctuation of the poloidal state does not produce flux noise. How to imprint the poloidal texture to a disordered spin system is a question for future research. Given that $\boldsymbol{F}_i$ is parallel to the magnetic field generated by the SC wire, it might be possible to at least partially polarize the spins in the poloidal direction using a large device current.

In conclusion, we predict novel methods for reducing flux noise in superconducting devices: We demonstrated with explicit numerical calculations that enhancing ferromagnetic correlation between wire surfaces, or engineering a poloidal spin texture allows the reduction of the flux noise power due to electron spins by several orders of magnitude. The remaining noise power, due to lattice nuclear spins, can be as much as 20 times smaller than the noise observed in the current state of the art devices.

* rdesousa@uvic.ca

[1] J. Clarke, *SQUIDs for Everything, an interview with Fabio Pulizzi*, Nat. Mater. **10**, 262 (2011).

[2] C. W. F. Everitt *et al.*, Phys. Rev. Lett. **106**, 221101 (2011).

[3] R.H. Koch, J. Clarke, W.M. Goubau, J.M. Martinis, C.M. Pegrum, and D. J. Van Harlingen, J. Low Temp. Phys. **51**, 207 (1983).

[4] F.C. Wellstood, C. Urbina, and J. Clarke, Appl. Phys. Lett. **50**, 772 (1987).

[5] F. Yoshihara, K. Harrabi, A.O. Niskanen, Y. Nakamura, and J.S. Tsai, Phys. Rev. Lett. **97**, 167001 (2006).

[6] R.C. Bialczak, R. McDermott, M. Ansmann, M. Hofheinz, N. Katz, E. Lucero, M. Neeley, A.D. O'Connell, H. Wang, A.N. Cleland, and J.M. Martinis, Phys. Rev. Lett. **99**, 187006 (2007).

[7] T. Lanting *et al.*, Phys. Rev. B **79** 060509 (2009).

[8] S.M. Anton, J.S. Birenbaum, S.R. O'Kelley, V. Bolkhovsky, D.A. Braje, G. Fitch, M. Neeley, G.C. Hilton, H.-M. Cho, K.D. Irwin, F.C. Wellstood, W.D. Oliver, A. Shnirman, and John Clarke, Phys. Rev. Lett. **110**, 147002 (2013).

[9] F. Yoshihara, Y. Nakamura, and J.S. Tsai, Phys. Rev. B **81**, 132502 (2010).

[10] F. Yan, J. Bylander, S. Gustavsson, F. Yoshihara, K. Harrabi, D.G. Cory, T.P. Orlando, Y. Nakamura, J.-S. Tsai, and W.D. Oliver, Phys. Rev. B **85**, 174521 (2012).

[11] J. Clarke and F.K. Wilhelm, Nature **453**, 1031 (2008).

[12] M. Stern, G. Catelani, Y. Kubo, C. Grezes, A. Bienfait, D. Vion, D. Esteve, and P. Bertet, Phys. Rev. Lett. **113**, 123601 (2014).

[13] D.H. Slichter, R. Vijay, S.J. Weber, S. Boutin, M. Boissonneault, J.M. Gambetta, A. Blais, and I. Siddiqi, Phys. Rev. Lett. **109**, 153601 (2012).

[14] S. Sendelbach, D. Hover, A. Kittel, M. Mück, J.M. Martinis, and R. McDermott, Phys. Rev. Lett. **100**, 227006 (2008).

[15] R.H. Koch, D.P. DiVincenzo, and J. Clarke, Phys. Rev. Lett. **98**, 267003 (2007).

[16] R. de Sousa, Phys. Rev. B **76**, 245306 (2007).

[17] L. Faoro and L.B. Ioffe, Phys. Rev. Lett. **100**, 227005 (2008).

[18] S.K. Choi, D.-H. Lee, S.G. Louie, and J. Clarke, Phys. Rev. Lett. **103**, 197001 (2009).

[19] Z. Chen and C.C. Yu, Phys. Rev. Lett. **104**, 247204 (2010).

[20] D. Lee, J.L. DuBois, and V. Lordi, Phys. Rev. Lett. **112**, 017001 (2014).

[21] T. Sleator, E.L. Hahn, C. Hilbert, and J. Clarke, Phys. Rev. Lett. **55**, 1742 (1985).

[22] M. Dubé and P. Stamp, Chem. Phys. **268**, 257 (2001).

[23] G. Rose and A.Y. Smirnov, J. Phys.: Condens. Matter **13**, 11027 (2001).

[24] J. Wu and C.C. Yu, Phys. Rev. Lett. **108**, 247001 (2012).

[25] T. Lanting, M.H. Amin, A.J. Berkley, C. Rich, S.-F. Chen, S. LaForest, and R. de Sousa, Phys. Rev. B **89**, 014503 (2014).

[26] W. Zhang and D.G. Cory, Phys. Rev. Lett. **80**, 1324 (1998).

[27] R. de Sousa, Topics Appl. Physics **115**, 183 (2009).

[28] J. Bylander, S. Gustavsson, F. Yan, F. Yoshihara, K. Harrabi, G. Fitch, D. G. Cory, Y. Nakamura, J.-S. Tsai, and W.D. Oliver, Nature Phys. **7**, 565 (2011).

[29] J. Atalaya, J. Clarke, G. Schön, and A. Shnirman, Phys. Rev. B **90**, 014206 (2014).

[30] A. De, Phys. Rev. Lett. **113**, 217002 (2014).

[31] C. Smithhisler, M. Kamon, L.M. Siveira and J. White, *FastHenry User's Guide Version 3.0* (Research Laboratory of Electronics, Department of Electrical Engineering and Computer Science, Massachusetts Institute of Technology, 1996).

[32] S.M. Anton, I.A.B. Sognnaes, J.S. Birenbaum, S.R. O'Kelley, C.J. Fourie, and John Clarke, Supercond. Sci. Technol. **26**, 075022 (2013).

[33] Chapter 4 in P.M. Chaikin and T.C. Lubensky, *Principles of condensed matter physics* (Cambridge University Press, Cambridge U.K., 2000).

[34] N.D. Mermin and H. Wagner, Phys. Rev. Lett. **17**, 1133 (1966).

[35] J.D. Jackson, *Classical Electrodynamics*, third edition (Wiley, New York, USA 1999).

[36] The flux-inductance theorem (proved in Section 5.17 of Ref. 35) states that $\Phi_i = \mathcal{H}_{\mathrm{mag}}/I_{\mathrm{SC}}$, where $\mathcal{H}_{\mathrm{mag}} = +\boldsymbol{\mu}_i \cdot \boldsymbol{B}(\boldsymbol{R}_i)$ is the total energy required to produce the spin-dipole configuration (including the energy necessary to create the spin, see Section 5.16 of Ref. 35). In Ref. 25 we missed a $-$ sign in the application of the flux-inductance theorem.

[37] E.H. Rhoderick and E.M. Wilson, Nature **194**, 1167 (1962).

[38] T. van Duzer and C.W. Turner, *Principles of superconductive devices and circuits* (Prentice Hall, New Jersey, USA 1999).

[39] V. Bouchiat, Supercond. Sci. Technol. **22**, 064002 (2009).

[40] L.C. Brown *et al.*, J. Chem. Phys. **24**, 751 (1956).

[41] R.E. Sheriff and D. Williams, Phys. Rev. **82**, 651 (1951).

[42] C.M. Baglin, Nuclear Data Sheets **80**, 1 (1997).

[43] S.S.P. Parkin, R. Bhadra, and K. P. Roche, Phys. Rev. Lett. **66**, 2152 (1991).